Journal of ELECTRONIC MATERIALS, Vol. 45, No. 3, 2016
DOI: 10.1007/s11664-015-4077-x

Simulation and Optimization of the Heat Exchanger for Automotive Exhaust-Based Thermoelectric Generators

C.Q. SU,[1,2,3] C. HUANG,[1] Y.D. DENG,[1] Y.P. WANG,[1] P.Q. CHU,[1] and S.J. ZHENG[1]

1.—Hubei Key Laboratory of Advanced Technology for Automotive Parts, Wuhan University of Technology, Wuhan 430070, China. 2.—Hubei Collaborative Innovation Center for Automotive Components Technology, Wuhan University of Technology, Wuhan 430070, China. 3.—e-mail: suchuqi@whut.edu.cn

In order to enhance the exhaust waste heat recovery efficiency of the automotive exhaust-based thermoelectric generator (TEG) system, a three-segment heat exchanger with folded-shaped internal structure for the TEG system is investigated in this study. As the major effect factors of the performance for the TEG system, surface temperature, and thermal uniformity of the heat exchanger are analyzed in this research, pressure drop along the heat exchanger is also considered. Based on computational fluid dynamics simulations and temperature distribution, the pressure drop along the heat exchanger is obtained. By considering variable length and thickness of folded plates in each segment of the heat exchanger, response surface methodology and optimization by a multi-objective genetic algorithm is applied for surface temperature, thermal uniformity, and pressure drop for the folded-shaped heat exchanger. An optimum design based on the optimization is proposed to improve the overall performance of the TEG system. The performance of the optimized heat exchanger in different engine conditions is discussed.

Key words: Heat exchanger, optimization, temperature uniformity, pressure drop

INTRODUCTION

For an internal combustion engine vehicle, about two thirds of the energy in fuel is released as heat and more than half of the waste heat is discharged through the exhaust pipe. With the development of thermoelectric materials, some of the thermal energy in automobile exhaust has the potential to be converted into electrical energy by using the thermoelectric generator (TEG).[1,2] As energy recovery from exhaust gases by TEG has low noise, high reliability, and zero emission, many studies have focused on applying TEG for automotive exhaust heat recovery. Yang et al.[2] reviewed several existing and potential automotive applications of thermoelectric technology including the waste heat recovery.

(Received June 2, 2015; accepted September 18, 2015; published online October 15, 2015)

Increasing ZT values of thermoelectric modules (TMs), improving the thermal performance of the heat exchanger, and optimizing the electrical topology of TMs are the major methods to enhance efficiency of automotive exhaust-based TEG.[3–5] Many researchers are interested in improving the efficiency of the TEG system. Espinosa et al.[6] developed a thermoelectric model using EES software based on a finite-difference method and a generator based on two kinds of thermoelectric materials, Mg_2Si/Zn_4Sb_3 and $Bi_2Te_3/(BiSb)_2Te_3$, was simulated. It was found that the width of the heat exchanger had a negative effect on the thermal difference ΔT applied to the thermoelectric material. The optimum proportion of the two thermoelectric materials was found for a real truck duty cycle. Kumar et al.[3,7] developed a numerical model to assess and optimize the performance of TEGs for waste heat recovery in automotive exhaust systems. It was found that, at the average inlet conditions, up to 64% of the inlet energy can be

transferred through the TMs and approximately 3.33% of the inlet power was converted into electrical power,[3] and four different topologies and parameters specific to the heat exchanger such as fin thickness, fin spacing, or the number of fins were investigated/optimized.[7] Chad Baker et al.[8] used a downhill simplex method to optimize the parameters that affected the electrical power output, including exhaust duct height, coolant duct height, fin spacing in the exhaust duct, location in the engine exhaust system, and number of flow paths within the constrained package volume. Lu et al.[9] tested the temperature distribution and pressure drop of three typical exhaust heat exchangers in different inlet temperature and mass flow rate. Niu et al.[10] analyzed the effects of exhaust channel size, number of channels, number of bafflers, baffler angle and engine operating condition on the heat, mass, and electric transfer characteristics and performance of engine exhaust-based TEG.

According to the above reviews of studies for the automotive exhaust-based TEG, most of the optimization of heat exchangers for waste heat recovery is limited to comparing several different cases of heat exchangers.[9–12] However, few studies did the parametric modeling for the heat exchanger and used an optimization algorithm to enhance the performance of the heat exchanger. To improve the temperature uniformity of a heat exchanger, Wang[13] firstly used a design of experiments (DOE), a surrogate model and multi-island genetic algorithms to optimize and design the fins distribution inside the heat exchanger.

In this study, a parametric modeling for the heat exchanger is developed. Response surface methodology (RSM) and a multi-objective genetic algorithm (MOGA) based on a central composite rotatable design (CCRD) is applied in optimization of the heat exchanger for automotive exhaust-based TEG.

MODEL DESCRIPTION

Geometric Model

When the TEG are located between the catalytic converter and the muffler, the heat exchanger obtained an ideal temperature uniformity, and the catalytic converter and muffler can keep working normally at the same time.[14] The inlet of the heat exchanger is connected to the outlet of the catalytic converter, and the muffler is behind the heat exchanger. Figure 1 presents a schematic diagram of the automotive exhaust-based TEG system. Sixty TMs are arranged uniformly on the top and bottom surface of a heat exchanger. The TMs hot side is in contact with heat exchanger surfaces, and the cold side is in contact with the coolant tank. The heat exchanger is integrated with the engine exhaust pipe, and the coolant tank is integrated with the engine cooling system.

In order to enhance the heat transfer performance and surface temperature uniformity, a three-segment heat exchanger with folded-shaped internal structure is developed.

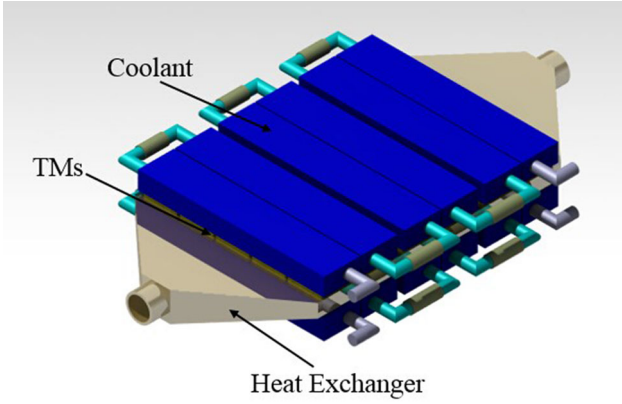

Fig. 1. Schematic of the TEG model.

As shown in Fig. 2, the heat exchange zone is divided into three segments, and each segment is 5 mm apart. N, $2N$, and $3N$ are the number of folded plates arranged in three segments from front to rear. More folded plates arranged in the rear can raise the surface temperature of the heat exchanger in the end. L_1, L_2, L_3 are the length of three segments of folded plates and D_1, D_2, D_3 are the thickness of the three segments of folded plates.

Since the heat exchanger model is symmetric, half the numerical model for the heat exchanger is developed by considering computational resources and efficiency. Limited by automobile chassis space, the shape of the heat exchanger makes it difficult for great changes. However, the internal structure of the heat exchanger does have a great impact on heat transfer performance and pressure drop,[4] and there is still much room to optimize the internal structure. Length and thickness of three segments of folded plates are done with parameterized modeling to facilitate further optimization.

Numerical Model

The CFD model of the heat exchanger is developed in the commercial code ANSYS 14.0; the flow and heat transfer is simulated in ANSYS CFX 14.0. When the engine operating conditions are constant, the temperature and flow rate of automobile exhaust can be approximately regarded as a steady-state. Considering exhaust is turbulence, a k–ε turbulence model is adopted to model its flow. For steady-state incompressible fluids, the transport equations for the k–ε model are:[15]

Turbulent kinetic energy equation:

$$\frac{\partial(\rho u_i k)}{\partial x_i} = \frac{\partial}{\partial x_i}\left[\left(\mu + \frac{\mu_t}{\sigma_k}\right)\frac{\partial k}{\partial x_i}\right] + P_k - \rho\varepsilon, \quad (1)$$

Turbulent energy dissipation rate equation:

$$\frac{\partial(\rho u_i \varepsilon)}{\partial x_i} = \frac{\partial}{\partial x_i}\left[\left(\mu + \frac{\mu_t}{\sigma_\varepsilon}\right)\frac{\partial \varepsilon}{\partial x_i}\right] + \frac{\varepsilon}{k}(C_{\varepsilon_1}P_k - C_{\varepsilon_2}\rho\varepsilon), \quad (2)$$

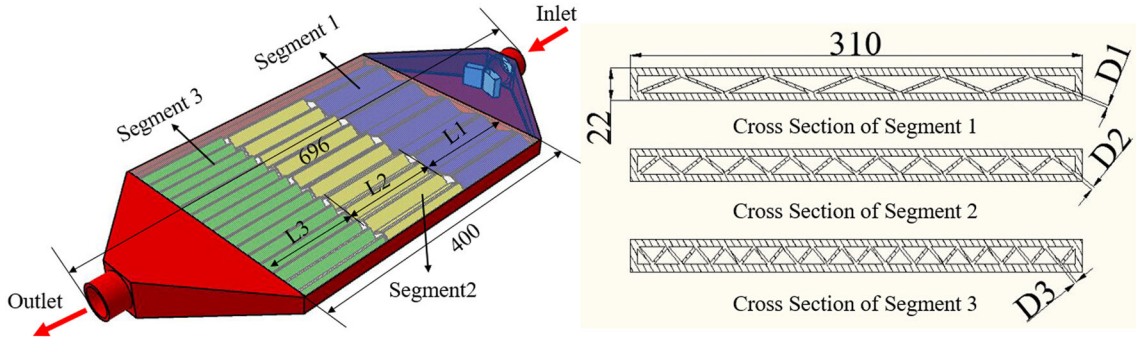

Fig. 2. Schematic of the heat exchanger model (unit: mm).

Turbulent viscosity:

$$\mu_t = C_\mu \rho \frac{k^2}{\varepsilon}, \tag{3}$$

Continuity equation:

$$\frac{\partial(\rho u_i)}{\partial x_i} = 0, \tag{4}$$

Momentum equation:

$$\frac{\partial(\rho u_i u_j)}{\partial x_i} = \frac{\partial}{\partial x_i}\left(\mu \frac{\partial u_j}{\partial x_i}\right) - \frac{\partial p}{\partial x_j}, \tag{5}$$

Energy equation:

$$\frac{\partial(\rho u_i t)}{\partial x_i} = \frac{\partial}{\partial x_i}\left(\frac{k}{C_p}\frac{\partial t}{\partial x_i}\right), \tag{6}$$

Empirical constant:

$$C_{\varepsilon_1} = 1.44, C_{\varepsilon_2} = 1.92, C_\mu = 0.09, \sigma_k = 1, \sigma_\varepsilon = 1.3, \tag{7}$$

where ρ is the density of exhaust, $u_i (i = 1, 2, 3)$ and $u_j (j = 1, 2, 3)$ is the velocity component, $x_i (i = 1, 2, 3)$ and $x_j (j = 1, 2, 3)$ is in rectangular coordinates, μ is the kinetic viscosity, μ_t is the turbulent eddy viscosity, k is the turbulence kinetic energy, ε is the turbulence energy dissipation rate, and P_k is the shear production of turbulent kinetic energy.

In order to reflect the test conditions more accurately, 0.03 kg/s mass flow with a temperature of 769 K and 5% turbulence intensity is applied at the inlet of fluid domain, outlet static pressure is set as 0, the surfaces in contact with TMs are set as a no-slip convection wall, and other outer surfaces are set as a no-slip adiabatic wall. The Simple algorithm is used to couple velocity, pressure, and temperature in this model.

OPTIMIZATION DESIGN

Optimization Objective

In order to increase the temperature and enhance uniformity, three sections of folded plates are arranged inside the heat exchanger. However, these folded plates will raise the pressure drop along the heat exchanger. Thus, balancing the temperature and pressure drop is a priority. To solve this issue, the number of three segments of folded plates N, $2N$, $3N$, the length of three segments of folded plates L_1, L_2, L_3 and the thickness of three segments of folded plates D_1, D_2, D_3, as shown in Fig. 2, are selected as variables. Limited by the total length of the heat exchanger, the sum of L_1, L_2 and L_3 is constant. So if L_1, L_2 is an independent variable, and L_3 is a driven variable.

In this study, to evaluate the temperature uniformity of the heat exchange area, the temperature uniformity coefficient γ is proposed:

$$\gamma = 1 - \frac{1}{n}\sum_{i=1}^{n} \frac{\sqrt{(T_i - T_{\text{mean}})^2}}{T_{\text{mean}}}, \tag{8}$$

where n is the number of TMs, T_i is temperature at ith TMs center, and T_{mean} is the average temperature of the heat exchange surface. When the temperature of all measurement points is the same, γ is equal to 1, which means the temperatures of heat transfer surfaces are the most uniform.

Pressure drop is defined as the difference between the inlet and outlet pressures of the heat exchanger. The pressure drop is calculated as follows:

$$P_{\text{drop}} = P_{\text{in}} - P_{\text{out}}, \tag{9}$$

where P_{drop} is the pressure drop along the heat exchanger, P_{in} is the inlet pressure, and P_{out} the outlet pressure.

Firstly, a different number of folded plates in three segments are considered to obtain a relatively ideal heat exchanger. Taking into account that the width of the heat exchanger is 310 mm, seven kinds of heat exchanger with a different number of folded plates are calculated, and the results are shown in Fig. 3. It can be observed that the average temperature and pressure drop both rise with increase of the number of folded plates, and they are conflictive.

The average temperature and pressure drop of the heat exchanger with 10, 20, 30 folded plates are balanced, and we will further optimize the length

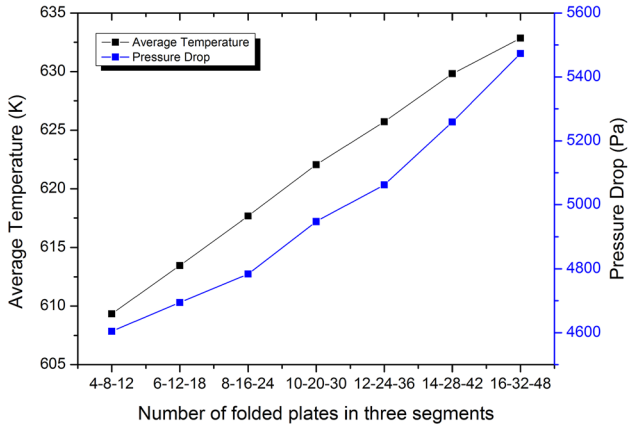

Fig. 3. Average temperature of the heat exchanger surface and pressure drop along the heat exchanger with a different number of the folded plates in three segments.

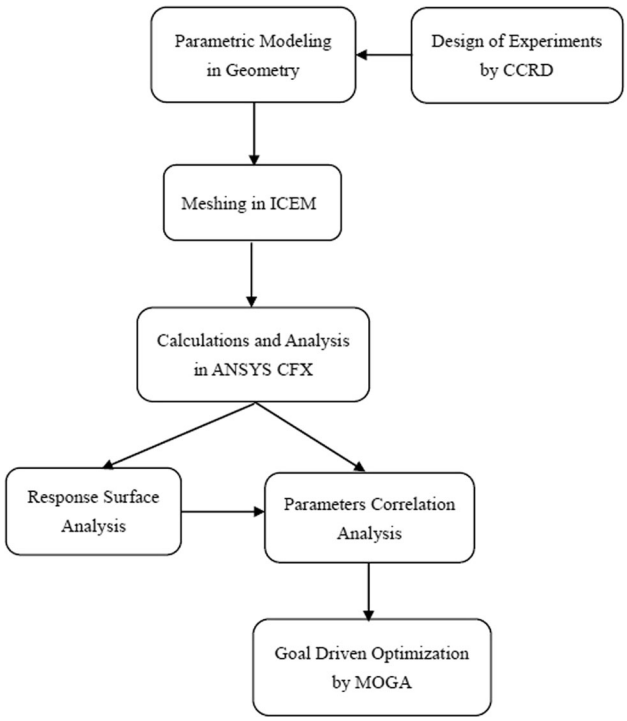

Fig. 4. Flowchart of optimization.

and thickness of three segments of folded plates in this heat exchanger.

By numerical simulation, the average surface temperature T_{mean}, temperature uniformity coefficient γ, and pressure drop P_{drop} are obtained to evaluate overall performance of the heat exchanger. The three objectives are considered for the goal driven optimization by MOGA based on the Response Surface model. The flowchart for optimization of the heat exchanger in the ANSYS WORKBNECH 14.0 is presented in Fig. 4.

Optimization Methods

RSM is a collection of statistical and mathematical methods that is applicable to analyze and optimize complex engineering problems. By experiments or simulation on a limited number of sample points in the design space, an approximate mathematical model of the response surface is developed.[16] RSM can greatly reduce the computational resource and numerical simulation in the optimization process.

The CCRD was first proposed by Box and Wilson,[17] Box and Hunter further developed CCRD.[18] Compared with the full factorial design, CCRD requires fewer experiments or simulations to effectively describe the steady-state process responses.[19] In this study, CCRD with five independent variables and five levels are used to design the experiments. The range of each variable and the actual level of variables are shown in Table I. Twenty-seven experimental runs and the corresponding results in CCRD are shown in Table II.

RESULTS AND DISCUSSION

Response Analysis

Based on the CFD results in CCRD, the response between the input parameter and the output parameter, which can be used to describe the interaction between different variables, is developed.

The average temperature of the heat exchanger surface in different lengths and thicknesses of the folded plates are presented in Fig. 5. The results show that the average temperature will be significantly reduced with an increase in length of the folded plates in segments 1 and 2, but higher average temperatures of the heat exchanger surface can be obtained with an increase in length of the folded plates in segment 3. Because the folded plates are ranged more densely in segment 3, and the flow rate of the exhaust gas will rise, then a higher convective heat transfer coefficient between exhaust gas and heat exchanger will be gained. The results also revealed that the temperature of the heat exchanger surface is not very sensitive to the thickness of the folded plates.

Figure 6 shows the response for the pressure drop along the heat exchanger against length and thickness of the folded plates in different segments. It can be observed that the pressure drop decreases with increases in length of the folded plates in segment 1 and segment 2. Conversely, the pressure drop will be increased with an increase in folded plates in segment 3. The thickness of the folded plates has a significant impact on the pressure drop. Otherwise, the pressure drop will rise significantly with increase in thickness of the folded plates.

The response relationship for temperature uniformity coefficient of the heat exchanger surface against the length and thickness of the folded plates in different segments is depicted in Fig. 7. An optimal length for the folded plates in each segment can

Table I. Range and actual levels of each variable

Variables	Lower bound	Upper bound	Levels				
			Lowest	Low	Center	High	Highest
L_1 (mm)	10	190	10	55	100	145	190
L_2 (mm)	10	190	10	55	100	145	190
L_3 (mm)	10	370	10	100	190	280	370
D_1 (mm)	1	3	1	1.5	2	2.5	3
D_2 (mm)	1	3	1	1.5	2	2.5	3
D_3 (mm)	1	3	1	1.5	2	2.5	3

$L_3 = 390 - L_2 - L_1$, *unit* mm, L_3 is a driven variable.

Table II. Design matrix and results in CCRD

Run	Input variable						Response variables		
	L_1 (mm)	D_1 (mm)	L_2 (mm)	D_2 (mm)	L_3 (mm)	D_3 (mm)	γ	T_{mean} (K)	P_{drop} (Pa)
1	100	2	100	2	190	2	0.91748	624.525	4998.58
2	10	2	100	2	280	2	0.896667	629.726	5081.87
3	190	2	100	2	100	2	0.916097	619.406	4917.15
4	100	1	100	2	190	2	0.91893	624.024	4932.73
5	100	3	100	2	190	2	0.917067	625.086	5065.63
6	100	2	10	2	280	2	0.913324	627.041	5030.22
7	100	2	190	2	100	2	0.909926	622.256	4936.12
8	100	2	100	1	190	2	0.91744	623.956	4900.71
9	100	2	100	3	190	2	0.917539	624.897	5112.34
10	100	2	100	2	190	1	0.911576	623.133	4781
11	100	2	100	2	190	3	0.921228	625.033	5364.45
12	55	1.5	55	1.5	280	2.5	0.908144	628.468	5196.09
13	145	1.5	55	1.5	190	1.5	0.920564	621.938	4759.83
14	55	2.5	55	1.5	280	1.5	0.9026	627.297	4865.88
15	145	2.5	55	1.5	190	2.5	0.924453	623.636	5103.71
16	55	1.5	145	1.5	190	1.5	0.906822	624.578	4797.5
17	145	1.5	145	1.5	100	2.5	0.917035	620.373	4974.13
18	55	2.5	145	1.5	190	2.5	0.910952	626.001	5134.67
19	145	2.5	145	1.5	100	1.5	0.912836	620.482	4792.35
20	55	1.5	55	2.5	280	1.5	0.90269	627.448	4946.84
21	145	1.5	55	2.5	190	2.5	0.925681	623.253	5157.5
22	55	2.5	55	2.5	280	2.5	0.906472	629.232	5370.18
23	145	2.5	55	2.5	190	1.5	0.91995	622.763	4946.68
24	55	1.5	145	2.5	190	2.5	0.911591	626.434	5241.68
25	145	1.5	145	2.5	100	1.5	0.914937	620.067	4869.37
26	55	2.5	145	2.5	190	1.5	0.905803	625.858	4993.14
27	145	2.5	145	2.5	100	2.5	0.917499	621.48	5139.62

be observed. Since the folded plates in segment 3 are denser, increasing the thickness of these folded plates can significantly increase the temperature uniformity coefficient.

Optimization Results

Based on the response between the factors and performance parameters, one hundred initial samples are screened to optimize the heat exchanger by MOGA. Three optimized candidates are shown in Table III. Considering the temperature of the heat exchanger surface and pressure drop along the heat exchanger, Candidate A is adopted. The temperature distribution of the initial heat exchanger and optimized heat exchanger is shown in Fig. 8. By optimization, the temperature on the rear surface of the heat exchanger significantly increases.

The optimization in this study is based on a steady inlet mass flow rate and temperature. However, the automotive operating condition often changes, the flow rate and temperature of the ex-

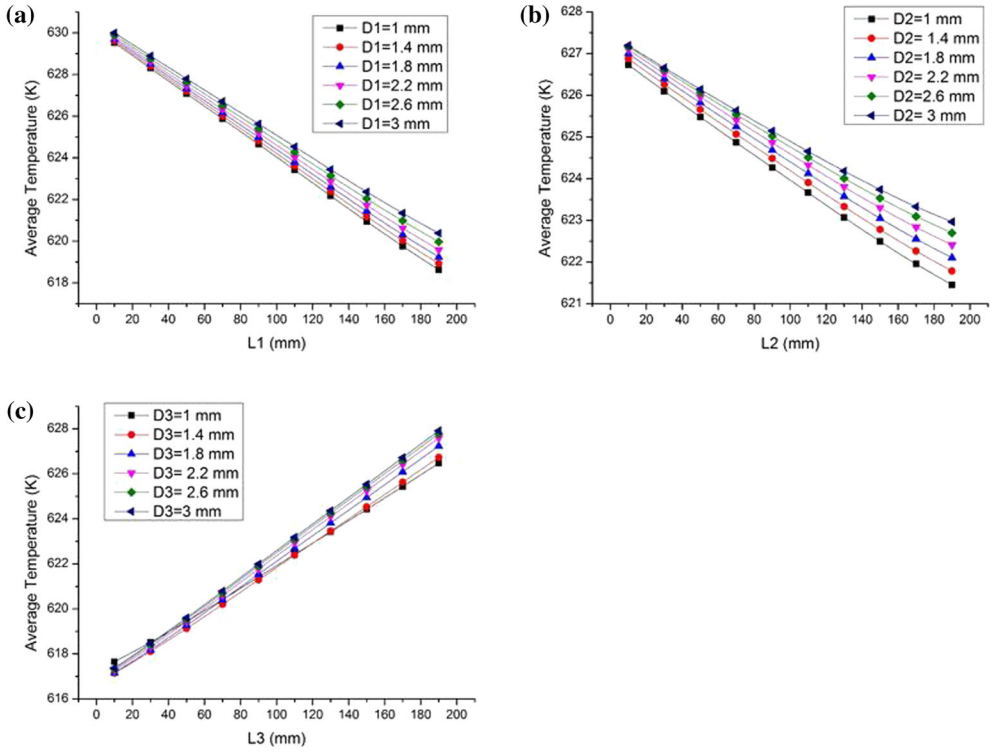

Fig. 5. Average temperature of the heat exchanger surface in different lengths and thicknesses of the folded plates in segment 1(a), segment 2(b), and segment 3(c).

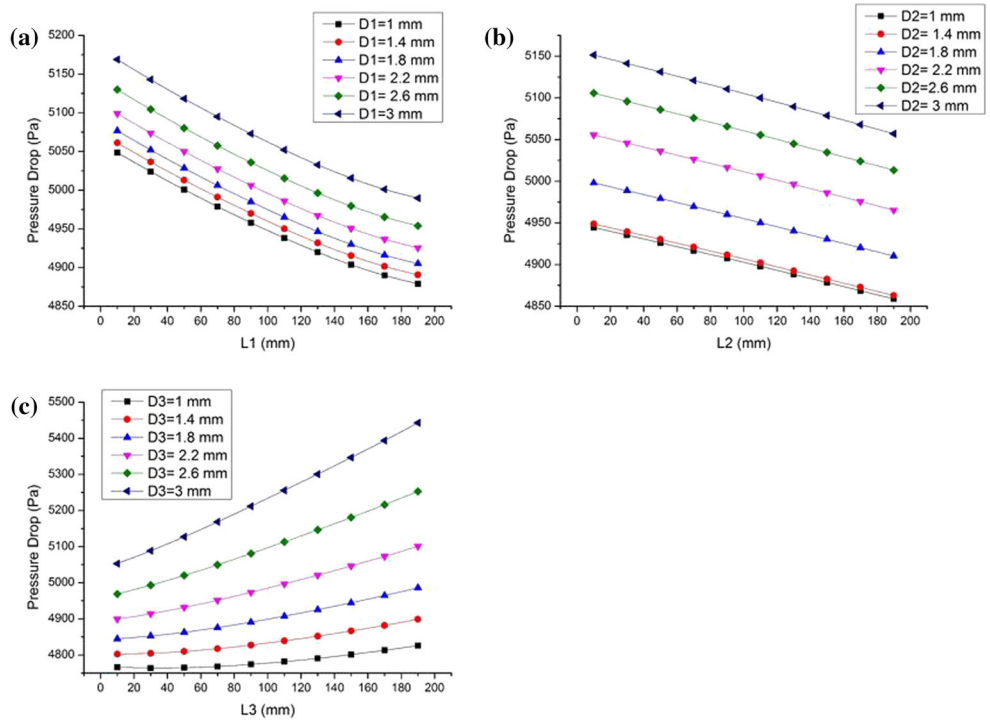

Fig. 6. Pressure drop along the heat exchanger in different lengths and thicknesses of the folded plates in segment 1(a), segment 2(b), and segment 3(c).

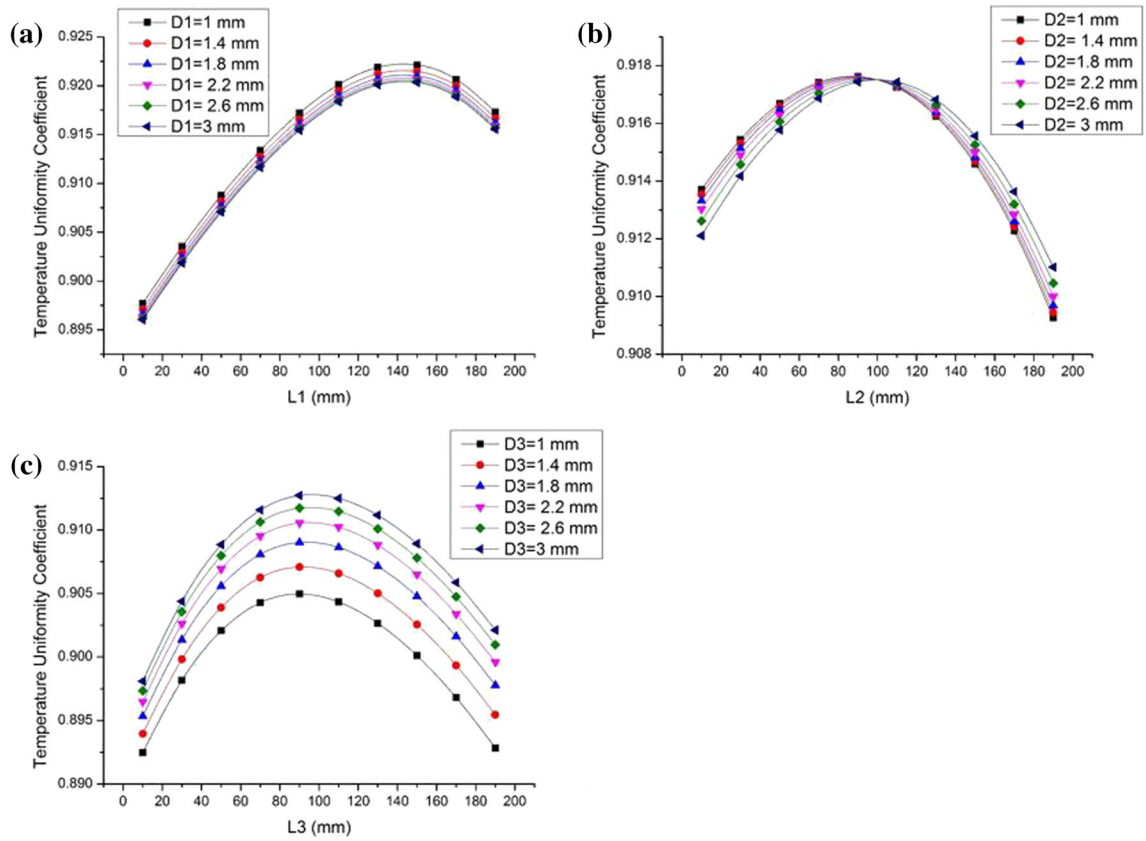

Fig. 7. Temperature uniformity coefficient of the heat exchanger surface in different lengths and thicknesses of the folded plates in segment 1(a), segment 2(b), and segment 3(c).

Table III. Candidate points of the optimization

Candidate points	L_1 (mm)	D_1 (mm)	L_2 (mm)	D_2 (mm)	L_3 (mm)	D_3 (mm)	γ	T_{mean} (K)	P_{drop} (Pa)
Candidate A	86.56	1.78	59.78	2.06	243.64	2.01	0.91	626.35	5023.30
Candidate B	156.7	1.11	11.64	1.53	221.65	2.35	0.92	623.36	5000.82
Candidate B	108.1	1.85	15.34	2.64	266.55	2.44	0.91	626.85	5266.10
Initial design	130	2	130	2	130	2	0.91	622.05	4947.40

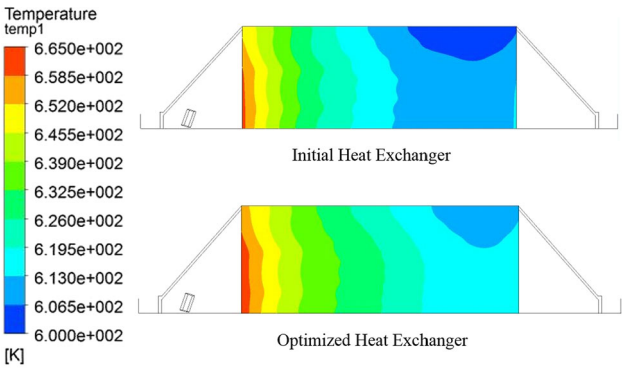

Fig. 8. Temperature distribution of the initial heat exchanger and optimized heat exchanger.

haust varies widely. The effect of inlet mass flow rate and temperature to the performance of the heat exchanger is further researched.

The relationship between the surface temperature of the heat exchanger and the inlet mass flow rate and temperature is shown in Fig. 9. It is observed that the average surface temperature and the inlet temperature are almost linear. At a low flow, the surface temperature increased rapidly with the increase of inlet mass flow rate.

Figure 10 describes the response for the pressure drop against the inlet mass flow rate and temperature. When the inlet mass flow rate is high, the pressure drop increases very significantly. It indicates that the high engine speed is not conducive to the heat exchanger. The inlet temperature also has

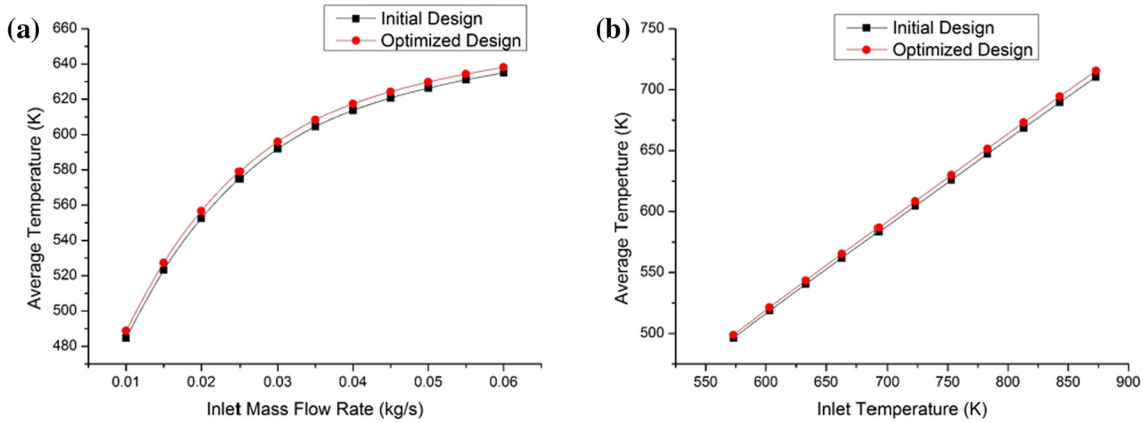

Fig. 9. Average temperature of heat exchanger surface in different inlet mass flow rates (a) and temperatures (b).

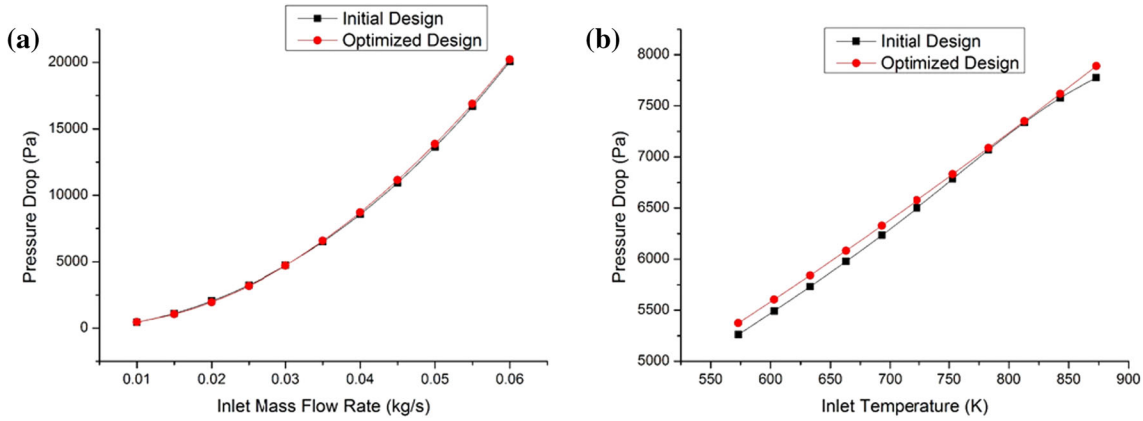

Fig. 10. Pressure drop along the heat exchanger in different inlet mass flow rates (a) and temperatures (b).

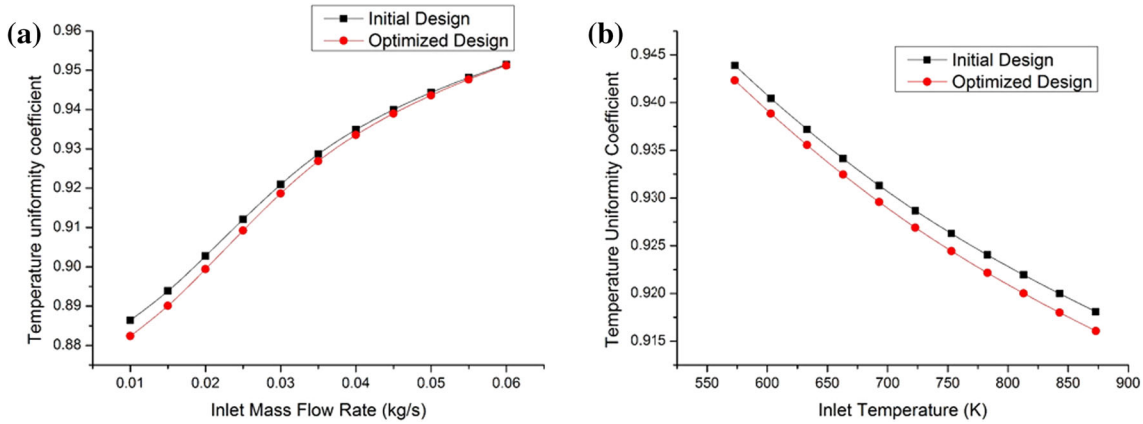

Fig. 11. Temperature uniformity coefficient of the heat exchanger surface in different inlet mass flow rates (a) and temperatures (b).

some influence on the pressure drop; a higher inlet temperature will cause a greater pressure drop.

The temperature uniformity coefficient of the heat exchanger surface in different inlet mass flow rates and temperatures is presented in Fig. 11. The temperature distribution of the heat exchanger surface will be more uniform with the increase of inlet mass flow rate. The temperature uniformity coefficient will decline with the inlet temperature increase.

CONCLUSION

Considering the surface temperature, pressure drop, and temperature uniformity as an optimization objective, a three-segment heat exchanger with

folded-shaped internal structure for the TEG system is optimized based on RSM and MOGA. The response relationship between the design variables and optimization objective is obtained and analyzed. The optimized heat exchanger with higher temperature distribution on the surface, few pressure drop increases, and the same temperature uniformity is finally obtained . Results show that the optimized structure of the heat exchanger is reasonable for automotive exhaust-based TEG systems. Results also confirm that RSM and MOGA are efficient optimization methods for heat exchanger design.

Heat transfer performance and pressure drop of the optimized heat exchanger in different engine conditions are investigated. Results show the optimized heat exchanger is not suitable for a high engine speed, since it will produce a huge pressure drop in the high inlet mass flow rate. Further optimization for the heat exchanger in different engine conditions is imperative. In this paper, internal structure of the heat exchanger is the focus of the research. However, the surface temperature and thermal uniformity of the heat exchanger are also affected by its dimension such as length, width, and height. Suitable dimensions of the TEG system may need to be calculated based on the displacement and power of the engine and different drive cycles in order to further improve the performance.

ACKNOWLEDGEMENTS

This work was funded by Grant No. 2013CB632505 from the National Basic Research Program of China (973 Program) and supported by the Fundamental Research Funds for the Central Universities (WUT142207005).

REFERENCES

1. A. Gabriel-Buenaventura and B. Azzopardi, *Renew. Sustain. Energy Rev.* 41, 955 (2015).
2. J. Yang and F.R. Stabler, *J. Electron. Mater.* 38, 1245 (2009).
3. S. Kumar, S.D. Heister, X. Xu, J.R. Salvador, and G.P. Meisner, *J. Electron. Mater.* 42, 665 (2013).
4. J. Esarte, G. Min, and D.M. Rowe, *J. Power Sources* 93, 72 (2001).
5. R. Quan, X. Tang, S. Quan, and L. Huang, *J. Electron. Mater.* 42, 1469 (2013).
6. N. Espinosa, M. Lazard, L. Aixala, and H. Scherrer, *J. Electron. Mater.* 39, 1446 (2010).
7. S. Kumar, S.D. Heister, X. Xu, J.R. Salvador, and G.P. Meisner, *J. Electron. Mater.* 42, 944 (2013).
8. C. Baker, P. Vuppuluri, L. Shi, and M. Hall, *J. Electron. Mater.* 41, 1290 (2012).
9. H. Lu, T. Wu, S. Bai, K. Xu, Y. Huang, W. Gao, X. Yin, and L. Chen, *Energy* 54, 372 (2013).
10. Z. Niu, H. Diao, S. Yu, K. Jiao, Q. Du, and G. Shu, *Energy Convers. Manag.* 85, 85 (2014).
11. X. Liu, Y.D. Deng, K. Zhang, M. Xu, Y. Xu, and C.Q. Su, *Appl. Therm. Eng.* 71, 364 (2014).
12. C.Q. Su, W.S. Wang, X. Liu, and Y.D. Deng, *Case Stud. Therm. Eng.* 4, 85 (2014).
13. Y. Wang, C. Wu, Z. Tang, X. Yang, Y. Deng, and C. Su, *J. Electron. Mater.* 44, 1724 (2015).
14. X. Liu, Y.D. Deng, S. Chen, W.S. Wang, Y. Xu, and C.Q. Su, *Case Stud. Therm. Eng.* 2, 62 (2014).
15. M. Hatami, D.D. Ganji, and M. Gorji-Bandpy, *Energy Convers. Manag.* 97, 26 (2015).
16. N. Aslan, *Fuel* 86, 769 (2007).
17. G.E.P. Box and K.B. Wilson, *J. R. Stat. Soc. B* 13, 1 (1951).
18. G.E.P. Box and J.S. Hunter, *Technometrics* 3, 311 (1961).
19. L. Sun and C.L. Zhang, *Int. J. Therm. Sci.* 75, 45 (2014).